The Future of EO-Enabled SDG 11.3.1 Monitoring Through Uncertainty-Aware Forecasting of Urban Land-Use Efficiency

Jojene Santillan
Caraga Center for Geo-Informatics & Department of Geodetic Engineering, College of Engineering and Geosciences
Caraga State University
Butuan City, Philippines

Mareike Dorozynski
Institute of Photogrammetry and GeoInformation
Leibniz University Hannover
Hannover, Germany
https://orcid.org/0000-0002-1293-6039

Christian Heipke
Institute of Photogrammetry and GeoInformation
Leibniz University Hannover
Hannover, Germany
https://orcid.org/0000-0002-7007-9549

Institute of Photogrammetry and GeoInformation
Leibniz University Hannover
Hannover, Germany
https://orcid.org/0000-0002-5895-8647

***Abstract*—Earth observation (EO) has become central to monitoring progress toward the Sustainable Development Goals (SDGs), particularly SDG Indicator 11.3.1, which assesses land-use efficiency (LUE) through the ratio of land consumption rate (LCR) to population growth rate (PGR). Current EO-based implementations remain predominantly retrospective and deterministic, relying on historical mappings of built-up area and population. However, decision-making for sustainable urban development increasingly requires forward-looking and uncertainty-aware information. This paper argues that the future of EO-enabled SDG monitoring lies in uncertainty-aware forecasting rather than deterministic retrospective assessment. We present a global EO-driven framework that integrates deep-learning-based forecasting of built-up area and population with Monte Carlo uncertainty propagation to derive probabilistic projections of SDG Indicator 11.3.1. Using multi-decadal EO-derived time series for 8,478 urban centres worldwide, we demonstrate how forecast uncertainty is structurally transmitted through SDG Indicator 11.3.1 and how deterministic forecasts can mask substantial uncertainty in future LUE classifications. The results highlight forecasting and uncertainty quantification as essential components of next-generation EO analytics for sustainable development.**

Keywords—Earth observation, SDG Indicator 11.3.1, land-use efficiency, uncertainty propagation, deep learning, urban forecasting

I. INTRODUCTION

Earth observation (EO) enables consistent, spatially explicit monitoring of urbanization. It underpins SDG Indicator 11.3.1, which measures land-use efficiency (LUE) as the ratio between the land consumption rate (LCR) and the population growth rate (PGR), also known as LCRPGR [1], [2]. Within this framework, efficiency is achieved when population growth occurs without disproportionate expansion of built-up land. To date, EO-based assessments of SDG 11.3.1 have mainly been retrospective, deriving deterministic indicator values from historical observations to analyze past urbanization patterns and trends (e.g., [3], [4], [5], [6]). While informative, such analyses offer limited guidance for future-oriented planning. Recent efforts have explored forward-looking assessments by combining scenario-based assumptions with regression models to project future LCRPGR values (e.g., [7], [8]). However, these approaches rely heavily on predefined scenarios rather than directly learning urban growth dynamics from EO time series.

In parallel, advances in deep learning (DL) have created new opportunities to forecast urban dynamics directly from EO-derived data. Time-series models based on convolutional networks, recurrent architectures such as Long Short-Term Memory (LSTM) and Gated Recurrent Units (GRU), and Transformers can capture nonlinear temporal dependencies and shared dynamics across collections of related time series [9], [10]. However, applications to urban growth forecasting remain limited, focusing primarily on population prediction (e.g., [11], [12], [13]). Jointly modeling built-up area (BUA) and population (Pop) from EO time series allows DL models to learn common temporal representations that improve generalization while maintaining contextual variability [14], [15], enabling coherent, large-scale forecasts of LCR, PGR, and LCRPGR. When formulated probabilistically, such models can also quantify forecast uncertainty, which is essential for ratio-based indicators such as SDG 11.3.1, where uncertainty in the input variables can propagate nonlinearly and lead to unstable indicator estimates.

Against this background, this paper advances uncertainty-aware forecasting as a core component of future EO-enabled SDG monitoring. Building on our earlier work[16], we extend an EO-driven framework that integrates DL-based time-series forecasting of urban dynamics with probabilistic uncertainty propagation for forward-looking assessment of SDG Indicator 11.3.1. The proposed framework transforms EO-derived BUA and Pop time series into predictive, uncertainty-aware SDG outputs, moving beyond retrospective and deterministic indicator computation. By jointly forecasting BUA and Pop and propagating uncertainty into indicator estimates, the framework enables future-oriented EO analytics for SDG monitoring [17], [18], [19]. In contrast to the original formulation, which relied on post-hoc uncertainty calibration, the present study streamlines the workflow by directly leveraging empirically well-calibrated predictive uncertainty produced by the forecasting models. The framework is further extended to support probabilistic LUE classification. Its application to global urban centres using multi-decadal EO time series demonstrates how explicit treatment of uncertainty fundamentally improves the interpretation of projected LUE outcomes.

This work was supported by the Philippine Department of Science and Technology–Science Education Institute (DOST-SEI) through a doctoral scholarship and by Caraga State University through a fellowship to J.S.

II. EO-Driven Forecasting and Uncertainty-Aware Indicator Framework

A. Joint Probabilistic Forecasting of BUA and Pop from EO Time Series

At the core of the framework is a probabilistic time-series forecasting model that jointly predicts BUA and Pop from EO-derived temporal data. Historical time series of these variables serve as inputs, enabling the model to learn shared urban dynamics across a large and diverse set of spatial units while ensuring internal consistency between land consumption and population change. Joint forecasting of BUA and Pop avoids incoherent indicator behavior that can arise when these variables are modeled independently.

B. Probabilistic Forecast Outputs and Uncertainty Representation

The forecasting model is formulated to produce probabilistic predictions of future BUA and Pop rather than deterministic point estimates. Forecast uncertainty is represented through predictive distributions that characterize the range of plausible future outcomes for both variables while preserving their joint behavior. This probabilistic representation provides a consistent basis for uncertainty propagation to SDG Indicator 11.3.1 and enables uncertainty-aware interpretation and classification of projected LUE outcomes.

C. Propagation of Forecast Uncertainty to SDG 11.3.1 Indicators

Uncertainty in the forecasts of BUA and Pop is explicitly propagated to the SDG Indicator 11.3.1 components using Monte Carlo simulation. For each spatial unit and forecast interval, a large number of joint realizations of BUA and Pop are sampled from their respective predictive distributions. For each joint realization, corresponding values of LCR, PGR, and their ratio (LCRPGR) are calculated using the standard SDG indicator 11.3.1 formulae (with t_1 and t_2 as the start and end years, and Δt as the interval length) [2]:

$$LCR = \frac{BUA_{t_2} - BUA_{t_1}}{BUA_{t_1}} \cdot \frac{1}{\Delta t} \quad (1)$$

$$PGR = \frac{ln\left(\frac{Pop_{t_2}}{Pop_{t_1}}\right)}{\Delta t} \quad (2)$$

This procedure yields probability distributions for each indicator component, rather than single-point estimates. Joint sampling is required to preserve the uncertainty dependence structure between BUA and Pop forecasts. This preservation is critical for ratio-based indicators such as SDG 11.3.1 because neglecting this dependence can lead to biased uncertainty bounds. By explicitly retaining both nonlinear transformations and inter-variable dependence, the resulting indicator distributions support uncertainty-aware interpretation of future LUE trajectories.

D. Probabilistic Classification of LUE

The probabilistic LCR, PGR, and LCRPGR outcomes are then translated into a probabilistic classification of LUE. Rather than assigning each spatial unit to a single efficiency class based on a point estimate (e.g., by using the mean or median forecasts of BUA and Pop in indicator calculations), classification is performed by evaluating the proportion of indicator realizations that fall within predefined LUE regimes, as defined by the signs and relative magnitudes of LCR and PGR and the resulting LCRPGR values (Table I). Each spatial unit is thus represented by a probability distribution across LUE classes, rather than a single categorical label. The most likely class is identified using the maximum posterior probability, while classification confidence is quantified using dominance probabilities. As illustrated in Fig. 1, a city may exhibit a 60% probability of efficient development, a 15% probability of inefficient expansion, and a 25% probability of inefficiency under demographic decline. Efficient growth is the most likely outcome, but it is not unequivocally dominant under forecast uncertainty. By moving from deterministic to probabilistic classification, the framework provides a more informative basis for interpretation and decision-making. It enables stakeholders to distinguish between robust efficiency outcomes and situations where multiple development regimes remain plausible, thereby aligning the interpretation of SDG 11.3.1 with risk-aware, forward-looking urban planning.

TABLE I. Land-use efficiency (LUE) classification under SDG Indicator 11.3.1, adapted from [20].

LUE Class	Logic / Interpretation
Efficient	Land consumption and population change are aligned, including cases where both increase proportionally (LCR > 0, PGR > 0, LCRPGR ≈ 1), population grows faster than land consumption (LCR > 0, PGR > 0, LCRPGR < 1), or both decline in a coordinated manner, with land contraction occurring at a rate comparable to or faster than population decline (LCR < 0, PGR < 0, LCRPGR ≈ 1 or > 1).
Inefficient Expansion (Sprawl-driven Inefficiency)	Built-up area expands faster than population growth (LCR > 0, PGR > 0, LCRPGR > 1) or expands despite stagnant population (LCR > 0, PGR ≈ 0; LCRPGR undefined), indicating land-intensive or sprawl-driven development.
Inefficient Under Demographic Decline	Population declines while land consumption expands or contracts insufficiently (LCR > 0 or ≈ 0, PGR < 0, LCRPGR < 0 or ≈ 0), leading to underutilization of built-up space and spatial oversupply.

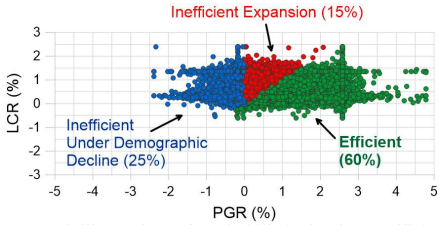

Fig. 1. Conceptual illustration of probabilistic land-use efficiency (LUE) classification for a hypothetical city. Each point represents one Monte Carlo realization of LCR and PGR derived from uncertainty-propagated built-up area and population estimates for the analysis period. Colored clusters indicate LUE regimes defined by the joint signs and relative magnitudes of LCR, PGR, and LCRPGR. Percentages denote the posterior probability of each class, calculated as the proportion of realizations falling within the corresponding regime.

III. Implementation and Application to Global Urban Centres

A. Dataset

The proposed framework was applied at scale to a global set of urban centres (UCs) using EO-derived time series of BUA and Pop. These data were used to generate probabilistic forecasts and projections for SDG Indicator 11.3.1 for the 2025–2030 period, aligning with the SDG target timeline. The analysis relied on the Global Human Settlement–Urban Centre Database (GHS-UCDB 2025), which provides globally consistent, multitemporal estimates of BUA and Pop for UCs [21]. UCs are defined as contiguous built-up areas with at least 50,000 inhabitants and a minimum density of 1,500 inhabitants per km² of built-up land. Contextual

attributes such as country, SDG region, and World Bank (WB) income group are also provided for each UC. From the original 11,422 UCs, a filtered subset of 8,478 UCs from our earlier work [16] was used, excluding cases with extreme annual change rates in BUA or Pop to ensure temporal consistency. The curated dataset was partitioned into geographically distinct training, validation, and test sets using stratified random sampling based on paired SDG region and WB income group, allocating approximately 70% of UCs to training (6,016) and 15% each to validation (1,263) and testing (1,119) (Fig. 2). All subsets share a common temporal coverage, with BUA and Pop time series spanning 1975–2020 at five-year intervals.

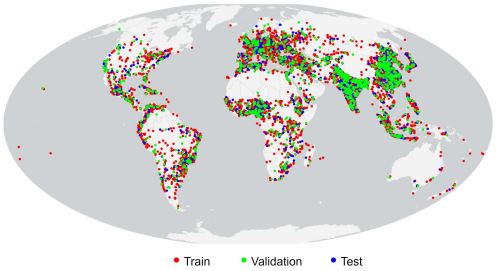

Fig. 2. Geographical distribution of 8,478 urban centres included in the study, showing the spatial allocation of the train, validation, and test sets used in model development.

B. Probabilistic Model Development and Evaluation

A DL–based approach was adopted to model the nonlinear, temporally structured relationships between BUA and Pop across a large and heterogeneous collection of UCs. EO-derived urban time series exhibit strong nonlinearity, scale heterogeneity, and cross-variable interactions that are difficult to capture consistently using linear or purely parametric models, particularly in a global setting. The global forecasting system was implemented using a GRU-based architecture within a deep ensemble formulation [22] to improve robustness and stability of probabilistic forecasts under stochastic training variability. Ensemble learning mitigates sensitivity to random initialization and optimization noise by aggregating predictions across independently trained models, yielding more reliable predictive performance and uncertainty estimates than single-model realizations [23], [24]. As as a dual-objective network, the model jointly forecasts BUA and Pop at two future time steps from EO-derived time series, where eight historical observations represent each UC. Owing to the limited temporal depth of the input data, the architecture was deliberately kept shallow to constrain model capacity and promote stable generalization across heterogeneous urban contexts. The GRU was selected based on its superior performance in preliminary benchmarking on the same dataset, relative to one-dimensional convolutional neural networks (Conv1D), LSTM, hybrid Conv1D+LSTM, and Conv1D+GRU, as well as Transformer-based models.

Temporal dynamics were encoded using a single unidirectional GRU layer with 128 units, which transforms the bivariate input sequence into a compact latent representation. This latent state was passed through a fully connected layer with 64 units and rectified linear unit (ReLU) activation to model nonlinear interactions between land consumption and population dynamics before projection to a multi-output layer producing forecasts for two future horizons. To operationalize the probabilistic formulation outlined in Section II.A, the model was trained using quantile loss [25] to estimate the 2.5th, 10th, 25th, 50th, 75th, 90th, and 97.5th conditional quantiles for each target variable and forecast horizon, which preserves distributional asymmetry and enables direct construction of empirical predictive distributions without imposing parametric assumptions. All architectural choices and training hyperparameters were selected through automated hyperparameter optimization using Optuna with Hyperband pruning [26], [27], with model development and training implemented in Python 3.10 using Keras and TensorFlow. The optimized configuration employed the Adam optimizer [28] with a learning rate of 10^{-3}, gradient clipping at 1.0, zero dropout in both recurrent and feedforward components, L2 regularization of 10^{-6}, and a batch size of 32. The training set of UCs, comprising observations from 1975 to 2010, was used for model fitting to predict two future time steps (2015 and 2020), while the validation set guided early stopping, pruning, and hyperparameter selection. To capture epistemic uncertainty, the optimized model configuration was retrained 30 times using different random weight initializations and data shuffling. These independently trained models formed a deep ensemble, with ensemble forecasts aggregated using a median-of-quantiles strategy to ensure coherence between point estimates and predictive intervals. Forecast performance was evaluated using two-horizon mean absolute error (MAE) and mean absolute percentage error (MAPE), both summarized as medians across all test set UCs. Probabilistic quality was assessed with respect to the nominal 95% prediction interval (0.95), defined by the 2.5th and 97.5th ensemble quantiles, using the prediction interval coverage probability (PICP) and the prediction interval average width (PIAW) to jointly evaluate calibration and sharpness [29].

C. SDG Indicator 11.3.1 Estimation, Uncertainty Propagation, and LUE Classification for 2025-2030

Ensemble-based probabilistic forecasts of BUA and Pop generated by the optimized GRU model were used to support uncertainty-aware estimation of SDG Indicator 11.3.1 for the 2025–2030 interval. For each UC, the predicted set of conditional quantiles for BUA and Pop was explicitly transformed into non-parametric empirical cumulative distribution functions (CDFs), which were subsequently treated as empirical marginal distributions for uncertainty propagation. These empirical CDFs were constructed by monotone interpolation between the estimated quantiles. The dependence between BUA and Pop forecast uncertainties was modeled using a copula-based framework [30], with copula modeling and model selection based on the correlations of validation-set forecast residuals. Based on Akaike Information Criterion (AIC) comparison, a level-2 truncated vine copula [31] composed of Student-t pair-copulas was selected and used to couple the forecasted BUA and Pop empirical marginal distributions. The fitted dependence structure primarily captured strong temporal dependence within BUA and Pop across forecast horizons, while cross-variable and higher-order conditional dependencies were weak and truncated to independence.

Joint Monte Carlo sampling (50,000 realizations per UC) from the coupled BUA–Pop distributions was propagated through the LCR, PGR, and LCRPGR formulations to obtain empirical distributions of SDG 11.3.1 outcomes. Probabilistic LUE classification (Table I) was then performed by assigning each Monte Carlo realization to a LUE regime and summarizing the frequencies of these regimes. Classification accuracy was first evaluated on the held-out test set for the 2015–2020 period using forecast-based SDG Indicator 11.3.1

estimates. This procedure was then applied to produce uncertainty-aware LUE projections for 2025–2030 for all 8,478 UCs. The posterior probability of the dominant regime was used as a classification confidence measure and discretized into five ordinal levels: very low (<0.50), low (0.50–0.65), moderate (0.65–0.80), high (0.80–0.95), and very high (>0.95). These ranges distinguish cases with no clear majority support (i.e., <0.50) from those with weak, moderate, strong, and near-deterministic regime dominance, providing an interpretable indication of sensitivity to uncertainty in forecasted BUA and Pop.

IV. Results and Discussion

On the held-out test set, the GRU ensemble achieved low forecast errors for BUA (median two-horizon MAE = 0.04 km²; median MAPE = 0.99%) and competitive accuracy for Pop (median MAE = 2,645 persons; median MAPE = 2.16%). The associated 95% prediction intervals were well-calibrated, achieving near-nominal coverage (BUA: PICP = 0.96; Pop: PICP = 0.95) with relatively sharp prediction intervals (BUA: median PIAW = 0.32 km²; Pop: median PIAW = 21,988 persons).

Table II illustrates the accuracy of the ensemble for probabilistic LUE classification for the 2015–2020 interval for the held-out test UCs. The accuracy metrics indicate a moderate overall agreement between observed and probabilistic LUE classifications (OA = 63.97%), demonstrating that uncertainty-aware forecasts provide informative but non-deterministic LUE outcomes. Class-specific accuracies indicate that some LUE regimes are more stable under forecast uncertainty than others, with higher PA and UA observed for the *Efficient and Inefficient Under Demographic Decline* classes, and substantially lower agreement for the *Inefficient Expansion* class. The confusion patterns suggest that misclassification is concentrated among specific regimes rather than being uniformly distributed, reflecting the differential sensitivity of LUE classes to uncertainty in BUA and Pop forecasts. For users of the framework, these results imply that probabilistic LUE outputs should be interpreted as varying in reliability across regimes, with some classifications providing robust signals and others indicating transitional or uncertain conditions where uncertainty-aware interpretation is essential.

Projected LUE classifications for 2025–2030 (Fig. 3a–b) show that *Inefficient Under Demographic Decline* is the dominant regime globally (55% of UCs), followed by *Efficient* LUE (42%), while *Inefficient Expansion* remains rare (2%). While the dominant class (Fig. 3a) provides a concise summary of the most likely LUE regime for each UC, the accompanying classification confidence (Fig. 3b) quantifies the stability of that assignment across Monte Carlo realizations. Confidence levels vary widely within the same dominant class, with most UCs falling into low to high confidence categories, and only a small fraction achieving very high confidence. This result indicates that projected outcomes are generally informative but seldom near-deterministic. Spatial patterns further show that UCs sharing the same dominant LUE regime may differ substantially in probabilistic support. In this sense, probabilistic LUE classification complements conventional, point-based LCRPGR analysis by distinguishing structurally stable regimes from those arising due to overlapping uncertainty in land consumption and population dynamics. Overall, the results demonstrate that uncertainty propagation affects not only the numerical stability of SDG 11.3.1 indicators but also the separability of the categorical LUE regimes derived from them, underscoring the need to interpret forecast-based LUE outcomes jointly in terms of dominant regime and the strength of probabilistic support.

TABLE II. CONFUSION MATRIX COMPARING OBSERVED AND PROBABILISTIC LUE CLASSIFICATIONS FOR 1,199 TEST URBAN CENTRES (2015–2020).

Predicted / Observed LUE Class	Efficient	Inefficient Expansion	Inefficient Under Demo-graphic Decline	Total	UA* (%)
Efficient	347	100	68	515	67.38
Inefficient Expansion	39	51	38	128	39.84
Inefficient Under Demographic Decline	87	100	369	556	66.37
Total	473	251	475	1199	
PA* (%)	73.36	20.32	77.68		
OA* (%)	63.97				

**PA: Producer's Accuracy; UA: User's Accuracy; OA: Overall Accuracy.*

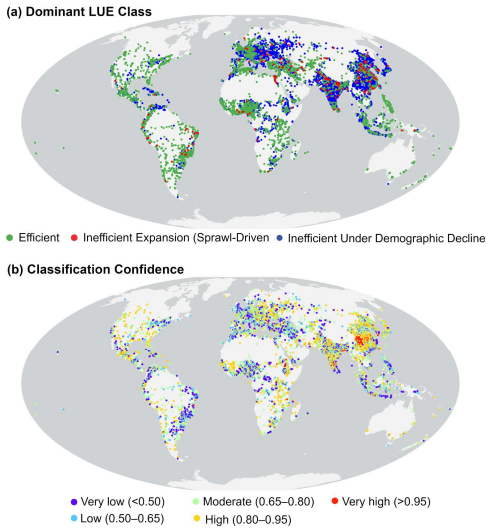

Fig. 3. Probabilistic LUE classification and classification confidence for the 2025–2030 period across 8,478 global urban centres.

V. Conclusions and Outlook

This study demonstrates that integrating EO-derived deep-learning-based forecasting of built-up area and population with Monte Carlo uncertainty propagation provides a robust framework for forward-looking assessment of SDG Indicator 11.3.1. By jointly forecasting BUA and Pop and explicitly propagating their uncertainty into LCR, PGR, and LCRPGR, the framework moves beyond deterministic, retrospective monitoring, enabling uncertainty-aware interpretation and classification of future LUE regimes. The results show that forecast uncertainty affects not only the magnitude of SDG 11.3.1 indicators but also the stability and separability of the derived LUE classes, highlighting the importance of probabilistic outputs for reliable interpretation. The framework is readily extensible to alternative EO data sources, longer forecast horizons, and region-specific implementations, and can support scenario analysis, policy evaluation, and risk-informed SDG monitoring. At a broader methodological level, the proposed EO-driven forecasting and uncertainty-aware indicator framework illustrates how uncertainty-aware EO analytics can enhance the interpretability and decision relevance of global sustainability indicators in the context of future urban development.

REFERENCES

[1] D. Ehrlich, S. Freire, M. Melchiorri, and T. Kemper, "Open and consistent geospatial data on population density, built-up and settlements to analyse human presence, societal impact and sustainability: a review of GHSL applications," *Sustainability*, vol. 13, no. 14, p. 7851, Jul. 2021, doi: 10.3390/su13147851.

[2] UN Statistics Division, "SDG indicator metadata (Harmonized metadata template – format version 1.0). Last updated 2025-04-23." Accessed: Oct. 05, 2025. [Online]. Available: https://unstats.un.org/sdgs/metadata/files/Metadata-11-03-01.pdf

[3] M. Melchiorri, M. Pesaresi, A. J. Florczyk, C. Corbane, and T. Kemper, "Principles and applications of the global human settlement layer as baseline for the land use efficiency indicator—SDG 11.3.1," *ISPRS International Journal of Geo-Information*, vol. 8, no. 2, 2019, doi: 10.3390/ijgi8020096.

[4] R. C. Estoque, M. Ooba, T. Togawa, Y. Hijioka, and Y. Murayama, "Monitoring global land-use efficiency in the context of the UN 2030 agenda for sustainable development," *Habitat International*, vol. 115, 2021, doi: 10.1016/j.habitatint.2021.102403.

[5] M. Schiavina, M. Melchiorri, C. Corbane, S. Freire, and F. Batista e Silva, "Built-up areas are expanding faster than population growth: regional patterns and trajectories in Europe," *Journal of Land Use Science*, vol. 17, no. 1, pp. 591–608, Jan. 2022, doi: 10.1080/1747423X.2022.2055184.

[6] J. R. Santillan and C. Heipke, "Assessing patterns and trends in urbanization and land use efficiency across the Philippines: a comprehensive analysis using global earth observation data and SDG 11.3.1 indicators," *PFG - Journal of Photogrammetry, Remote Sensing and Geoinformation Science*, 2024, doi: 10.1007/s41064-024-00305-y.

[7] H. Jiang *et al.*, "Projections of urban built-up area expansion and urbanization sustainability in China's cities through 2030," *Journal of Cleaner Production*, vol. 367, 2022, doi: 10.1016/j.jclepro.2022.133086.

[8] C. Wang *et al.*, "Is the assessment approach of Sustainable Development Goal 11.3.1 justified? Evidence from the drivers of future urban land use efficiency," *Journal of Cleaner Production*, vol. 444, p. 141147, Mar. 2024, doi: 10.1016/j.jclepro.2024.141147.

[9] K. Benidis *et al.*, "Deep learning for time series forecasting: tutorial and literature survey," *ACM Comput. Surv.*, vol. 55, no. 6, pp. 1–36, Jul. 2023, doi: 10.1145/3533382.

[10] W. Li and K. L. E. Law, "Deep learning models for time series forecasting: a review," *IEEE Access*, vol. 12, pp. 92306–92327, 2024, doi: 10.1109/ACCESS.2024.3422528.

[11] N. Alghanmi, R. Alotaibi, S. Alshammari, and A. Mahmood, "Population fusion transformer for subnational population forecasting," *Int J Comput Intell Syst*, vol. 17, no. 1, p. 26, Feb. 2024, doi: 10.1007/s44196-024-00413-y.

[12] C. Geiß, J. Maier, E. So, and Y. Zhu, "LSTM models for spatiotemporal extrapolation of population data," in *2023 Joint Urban Remote Sensing Event (JURSE)*, Heraklion, Greece: IEEE, May 2023, pp. 1–4. doi: 10.1109/JURSE57346.2023.10144145.

[13] I. Grossman, T. Wilson, and J. Temple, "Forecasting small area populations with long short-term memory networks," *Socio-Economic Planning Sciences*, vol. 88, p. 101658, Aug. 2023, doi: 10.1016/j.seps.2023.101658.

[14] P. Montero-Manso and R. J. Hyndman, "Principles and algorithms for forecasting groups of time series: locality and globality," *International Journal of Forecasting*, vol. 37, no. 4, pp. 1632–1653, Oct. 2021, doi: 10.1016/j.ijforecast.2021.03.004.

[15] A.-A. Semenoglou, E. Spiliotis, S. Makridakis, and V. Assimakopoulos, "Investigating the accuracy of cross-learning time series forecasting methods," *International Journal of Forecasting*, vol. 37, no. 3, pp. 1072–1084, Jul. 2021, doi: 10.1016/j.ijforecast.2020.11.009.

[16] J. R. Santillan, M. Dorozynski, and C. Heipke, "A deep learning framework for forecasting built-up area and population to support land use efficiency projections under SDG 11.3.1," *ISPRS Annals of the Photogrammetry, Remote Sensing and Spatial Information Sciences*, vol. in press, 2025.

[17] B. Ferreira, M. Iten, and R. G. Silva, "Monitoring sustainable development by means of earth observation data and machine learning: a review," *Environ Sci Eur*, vol. 32, no. 1, p. 120, Dec. 2020, doi: 10.1186/s12302-020-00397-4.

[18] C. Persello *et al.*, "Deep learning and earth observation to support the sustainable development goals: current approaches, open challenges, and future opportunities," *IEEE Geosci. Remote Sens. Mag.*, vol. 10, no. 2, pp. 172–200, Jun. 2022, doi: 10.1109/MGRS.2021.3136100.

[19] Q. Zhao and L. Yu, "Advancing sustainable development goals through earth observation satellite data: current insights and future directions," *J Remote Sens*, vol. 5, p. 0403, Jan. 2025, doi: 10.34133/remotesensing.0403.

[20] J. Santillan, M. Dorozynski, and C. Heipke, "Enhancing land use efficiency assessment through built-up area–built-up volume trajectories: integrating vertical urban growth into SDG 11.3.1 monitoring," *IJGI*, vol. 14, no. 10, p. 404, Oct. 2025, doi: 10.3390/ijgi14100404.

[21] European Commission *et al.*, "Stats in the City the GHSL Urban Centre Database 2025," Publications Office of the European Union, Luxembourg, 2024. doi: https://data.europa.eu/doi/10.2760/3046391.

[22] B. Lakshminarayanan, A. Pritzel, and C. Blundell, "Simple and scalable predictive uncertainty estimation using deep ensembles," in *Advances in Neural Information Processing Systems 30 (NIPS 2017)*, 2017.

[23] X. Dong, Z. Yu, W. Cao, Y. Shi, and Q. Ma, "A survey on ensemble learning," *Front. Comput. Sci.*, vol. 14, no. 2, pp. 241–258, Apr. 2020, doi: 10.1007/s11704-019-8208-z.

[24] M. A. Ganaie, M. Hu, A. K. Malik, M. Tanveer, and P. N. Suganthan, "Ensemble deep learning: a review," *Engineering Applications of Artificial Intelligence*, vol. 115, p. 105151, Oct. 2022, doi: 10.1016/j.engappai.2022.105151.

[25] Y. Wang, D. Gan, M. Sun, N. Zhang, Z. Lu, and C. Kang, "Probabilistic individual load forecasting using pinball loss guided LSTM," *Applied Energy*, vol. 235, pp. 10–20, Feb. 2019, doi: 10.1016/j.apenergy.2018.10.078.

[26] T. Akiba, S. Sano, T. Yanase, T. Ohta, and M. Koyama, "Optuna: a next-generation hyperparameter optimization framework," in *Proceedings of the 25th ACM SIGKDD International Conference on Knowledge Discovery & Data Mining*, Anchorage AK USA: ACM, Jul. 2019, pp. 2623–2631. doi: 10.1145/3292500.3330701.

[27] L. Li, K. Jamieson, G. DeSalvo, A. Rostamizadeh, and A. Talwalkar, "Hyperband: a novel bandit-based approach to hyperparameter optimization," *Journal of Machine Learning Research*, vol. 18, no. 185, pp. 1–52, 2018.

[28] D. P. Kingma and J. Ba, "Adam: a method for stochastic optimization," in *3rd International Conference on Learning Representations (ICLR).*, 2015.

[29] V. Jensen, F. M. Bianchi, and S. N. Anfinsen, "Ensemble conformalized quantile regression for probabilistic time series forecasting," *IEEE Trans. Neural Netw. Learning Syst.*, vol. 35, no. 7, pp. 9014–9025, Jul. 2024, doi: 10.1109/TNNLS.2022.3217694.

[30] R. B. Nelsen, *An Introduction to Copulas*, Second Edition. New York, USA: Springer Science+Business Media, Inc., 2006.

[31] T. Nagler, "Simplified vine copula models: state of science and affairs," *Risk Sciences*, vol. 1, p. 100022, 2025, doi: 10.1016/j.risk.2025.100022.